Controller Design of an Electric Power Steering System

Dongwook Lee, Kyung-Soo Kim, *Member, IEEE*, and Soohyun Kim

***Abstract*— This brief presents a new method of analyzing stability and design of a controller for an electric power steering (EPS) system. The most important task when designing a steering system is ensuring that the driver is pleased with how the steering feels. The way that the steering feels is dependent upon the assist torque map. The assist torque map is a one-to-one map between sensed driver torque and assist motor torque that varies with the cars speed. However, an assist torque map cannot be applied alone as an EPS controller because of high level of steering assist gain and nonlinearity of the torque map. Both elements of torque map can result in instability, which leads to vibration or divergence of the steering system. Therefore, an EPS system always needs to be designed with a stabilizing compensator and an assist torque map. The objective of designing a compensator is to stabilize the system with robustness and attenuate any unpleasant vibration. This brief presents a mechanical model of the EPS system and demonstrates a method to identify the model parameter. Based on the EPS model, stability of the system with an approximate linear torque map and nonlinear torque map is analyzed. Furthermore, criteria for designing the stabilizing compensator are suggested. Lead-lag compensators with different parameters are applied with the torque map in simulations, and vehicle experiments are performed to verify the theoretical analysis.**

***Index Terms*— Controller design, electric power steering (EPS), stability analysis, system nonlinearity.**

I. Introduction

ELECTRIC power steering (EPS) is a motor-supported power steering system that helps provide the driver with a lightweight and convenient steering feel. Today, most passenger cars are equipped with an EPS system to support the driver instead of a hydraulic power steering system due to its many advantages [1]. These advantages include high fuel efficiency, a compact volume, a steering feel with easy tuning, and the ability to combine the system with other electrically controlled systems in the vehicle, such as the electric stability control.

A torque map is the main element of an EPS controller; it determines how much steering torque is assisted by the motor. The torque map provides a nonlinear increasing function between the measured driver torque and assist torque from the motor. The shape of the torque map determines how the steering feels for the driver [2]. Generally, the slope of the torque map is the steepest when the velocity is zero, and then decreases with an increase in speed, because the torque that is needed to steer is the largest when the vehicle is parked, and the steering needs to feel heavier for the driver when a vehicle is going fast to achieve stability. A high level of controller gain at low velocity and the nonlinearity of the torque map can be a source of instability and vibration in the system [3], [8]; therefore, the stabilizing compensator is required in addition to the torque map to complete the EPS controller. However, designing a proper controller for an EPS has become a challenging problem for a number of reasons [4]. The controller needs to be robust in case that there are any unmodeled dynamics and parameter uncertainty. The parameter adjustment can be challenging, because even for the same type of vehicle, each car can have some variation in its system parameters. In addition, because the steering system interacts with human hands, which can be sensitive, a good controller design should eliminate undesirable vibrations.

There have been many studies suggesting various forms of EPS controllers to make the system stable. Reference [5] suggested stable conditions based on an EPS model and utilized a fixed-structure compensator to stabilize the system and minimize the torque vibration. Reference [6] used a frequency-weighted damping compensator to increase the phase margin of the system, but the increased range of the phase margin was restricted. Reference [7] employed a H-infinity control to assist torque, improve the steering feel, and enhance the closed-loop robustness. The limitation is that the proposed H-infinity control has a very high order and cannot eliminate vibrations. Reference [8] suggested a robust integral sliding-mode controller to generate the assist torque, stabilize the system, and improve the EPS damping characteristics. Reference [9] proposed an optimal linear-quadratic regulator controller for a dual-pinion EPS.

Previous research concerning EPS controller design has some limitations. First, most studies approximate the nonlinear torque map as a simple linear gain and do not analyze the influence of nonlinearity on stability of the system. Linearized system only represents dynamic characteristic in the neighborhood of an operating point, and nonlinear elements of system often cause unique phenomena, which cannot be occurred in the linear system. Even though linearized system is stable, nonlinear element such as torque map can cause instability, which is directly connected to divergence or severe vibration of system. Second, the proposed controllers were only verified with simulation or bench tests. Simulations and bench tests are very restricted environments and do not reflect all characteristics of an actual vehicle. Computer simulation does not express the unmodeled dynamics of the system. In addition, in simulation and bench test environments, it is hard to recreate the reaction force from the road through the

Manuscript received December 15, 2016; accepted February 20, 2017. Manuscript received in final form March 2, 2017. Recommended by Associate Editor K. Butts.

The authors are with the Department of Mechanical Engineering, Korea Advanced Institute of Science and Technology, Daejeon 305-701, South Korea (e-mail: kyungsookim@kaist.ac.kr).

Color versions of one or more of the figures in this paper are available online at http://ieeexplore.ieee.org.

Digital Object Identifier 10.1109/TCST.2017.2679062

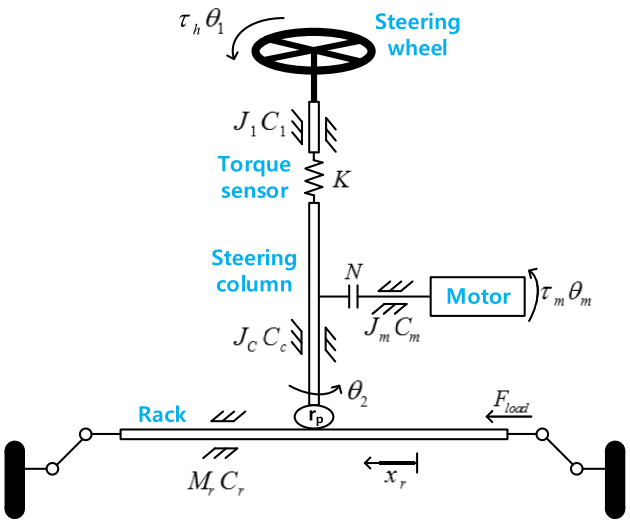

Fig. 1. EPS system model.

tires. The tire reaction force is hard to model because of the dramatic nonlinear characteristics of the tires [10]. This is especially apparent when the vehicle is in park, which is the worst case for system stability because of the large assist gain. Last, many researchers suggested too complex controllers to be implemented at practical use. Large computational effort is strongly avoided in the development of a commercial vehicle.

This brief presents a new way of analyzing the stability of an EPS system with a nonlinear torque map and suggests the whole process to design a stabilizing compensator for the given torque map. The EPS system is modeled as two lumped masses connected with a torsional spring and a model parameter identification method is also suggested. The effects of two potential source of instability, large gain and nonlinearity of torque map, are analyzed in the Laplace domain separately, and each gives criterion for designing a stabilizing compensator. A lead-lag compensator is employed as a stabilizing compensator for loop shaping in the frequency domain and design method to select parameters of compensator is also suggested. Finally, simulations and vehicle experimental results are examined to verify the theoretical analysis.

II. EPS System Modeling and Identification

A. EPS System Model

There are three types of EPS systems according to location of motor attachment: column-type, pinion-type, and rack-type. For research purposes, we have chosen the column-type EPS system; its dynamic model is shown in Fig. 1. The meaning of each parameter and variable shown in the figure and throughout this text is defined in Table I. The EPS dynamic model consists of four masses: the steering wheel, the column, the motor, and the rack. The steering wheel and the column are connected by a torque sensor that contains an elastic torsion bar, and the motor and the rack are connected to the column by the worm gear and the pinion, respectively. According to Newton's second law of motion, the equations for the motion of each mass can be observed in the following (1)–(4).

TABLE I
Model Parameters and Variables

Notation	Description
J_1	Moment of inertia of steering wheel
C_1	Damping coefficient of steering wheel
J_c	Moment of inertia of column
C_c	Damping coefficient of column
K	Torsional stiffness of torque sensor
M_r	Mass of rack
C_r	Damping coefficient of rack
J_m	Moment of inertia of motor
C_m	Damping coefficient of motor
θ_1	Steering wheel angle
θ_2	Column angle
θ_m	Motor angle
x_r	Rack displacement
τ_h	Driver torque
τ_m	Motor torque
F_{load}	Load force of rack from tire
i_q	q-axis current
K_m	Motor constant between q-axis current and assist torque(τ_a)
r_p	Pinion radius
N	Gear ratio

Equation (5) represents the gear ratios of the rack and pinion and the worm gear

$$J_1\ddot{\theta}_1 + C_1\dot{\theta}_1 + K(\theta_1 - \theta_2) = \tau_h \tag{1}$$
$$J_c\ddot{\theta}_2 + C_c\dot{\theta}_2 + K(\theta_2 - \theta_1) = \tau_{\text{gear}} - \tau_{\text{pinion}} \tag{2}$$
$$J_m\ddot{\theta}_m + C_m\dot{\theta}_m = \tau_m - \tau_{\text{gear}}/N \tag{3}$$
$$M_r\ddot{x_r} + C_r\dot{x}_r = \tau_{\text{pinion}}/r_p - F_{\text{load}} \tag{4}$$
$$r_p\theta_2 = x_r,\ N\theta_2 = \theta_m. \tag{5}$$

Equations (2)–(4) can be integrated to one lumped mass equation (6) and simplified with the equivalent moment of inertia and a damping coefficient

$$J_2\ddot{\theta}_2 + C_2\dot{\theta}_2 + K(\theta_2 - \theta_1) = \tau_a - \tau_l \tag{6}$$
$$J_2 = J_c + N^2J_m + r_pM_r, \quad C_2 = C_c + N^2C_m + r_pC_r$$
$$\tau_a = N\tau_m, \quad \tau_l = r_pF_{\text{load}}. \tag{7}$$

J_2 and C_2 represent the equivalent moment of inertia and damping coefficient of the lumped mass and τ_a and τ_l represent equivalent assist torque and load torque.

Furthermore, (8) and (9) describe the measured torque at the torque sensor and the assist motor torque reference calculated at the controller

$$\tau_s = K(\theta_1 - \theta_2) \tag{8}$$
$$\tau_{a,\text{ref}} = h(\tau_s) \tag{9}$$

$h(\tau_s)$ represents controller containing nonlinear torque map and compensator.

Every actuator has its own bandwidth; therefore, the motor dynamics can be expressed as a low-pass filter with cutoff

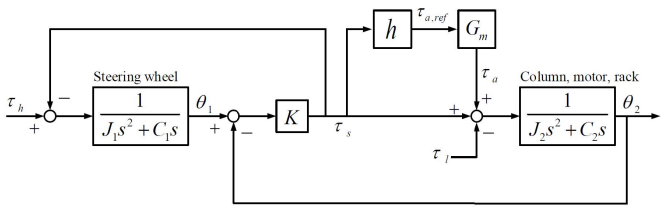

Fig. 2. Block diagram of the EPS system.

TABLE II
SYSTEM IDENTIFICATION EXPERIMENTAL CONDITIONS

Singal type	Sine function
Amplitude	5, 7, 9 Nm
Frequency	$f = a_0 r^{i-1},\ i = 1, 2...51$
a_0	1 Hz
r	1.0615
K_m	0.8764

frequency ω_m

$$\frac{\tau_a}{\tau_{a,\text{ref}}} = \frac{\omega_m}{s+\omega_m} = G_m(s). \tag{10}$$

Fig. 2 shows a block diagram of the entire EPS system, which describes the flows of the system from external inputs (driver torque and road disturbance) to system states (handle and column angle).

B. Model Parameter Identification

A model-based controller always needs a system identification to determine the value of the model parameter. The method used for exact system identification is as important as developing a good system model. This is because a good model for a controller design is useless without the modeling parameter values.

To identify the parameter values, we compare the system response of the motor excitation of various frequencies with the system transfer function from model. Vehicle is given lift-on and free-handle conditions to ensure no external torque other than the motor torque ($\tau_l = 0$ and $\tau_h = 0$). With these conditions, the motor excites the system with sine input with various frequencies, and the column angle, the motor current, and the torque sensor value are all measured as system output variables. The experimental conditions are expressed in Table II. By modifying (1) and (6) with lift-on ($\tau_l = 0$) and free-handle conditions ($\tau_h = 0$), we can obtain a transfer function from the assist torque to the column angle and torque sensor and from the torque sensor to the column angle, as observed in (11)–(13)

$$\frac{\theta_2}{i_q} = \frac{K_m(J_1 s^2 + C_1 s + K)}{(J_1 s^2 + C_1 s + K)(J_2 s^2 + C_2 s + K) - K^2} \tag{11}$$

$$\frac{\tau_s}{i_q} = \frac{K_m K(J_1 s^2 + C_1 s)}{(J_1 s^2 + C_1 s + K)(J_2 s^2 + C_2 s + K) - K^2} \tag{12}$$

$$\frac{\theta_2}{\tau_s} = \frac{J_1 s^2 + C_1 s + K}{K(J_1 s^2 + C_1 s)}. \tag{13}$$

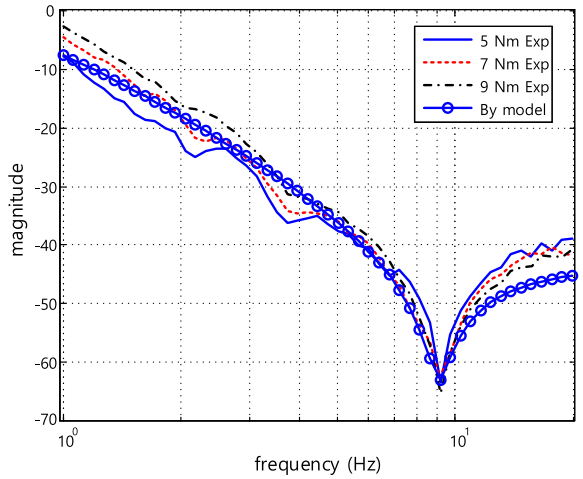

Fig. 3. Bode plot of the magnitude of θ_2/τ_s from the experimental results and the transfer function.

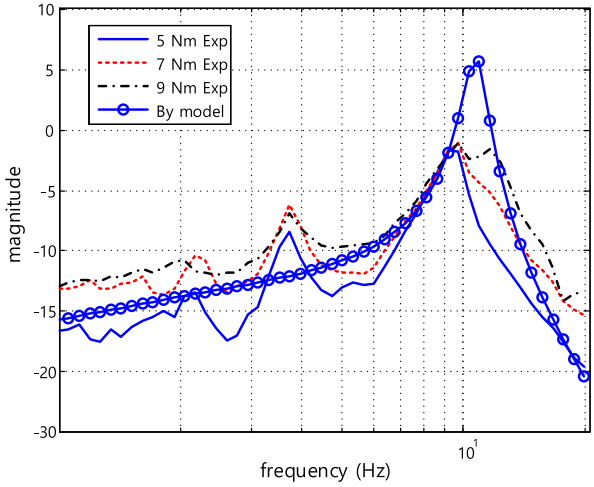

Fig. 4. Bode plot of the magnitude of τ_s/τ_a from the experimental results and the transfer function.

Equation (13) only contains parameters J_1, C_1, and K; therefore, if we know K from the sensor specification, we can find the value of J_1, and C_1, which will then minimize the sum of square error between the transfer function (11) and the experimental result for each frequency

$$\text{Find } \mathrm{J}_1, C_1 \text{ s.t. } \min e = \sum_i [\text{Amp}_{\text{exp}}(\omega_i) - \text{Amp}_{\text{model}}(\omega_i)]^2.$$

Then, based on the values of J_1, C_1, and K, we can find the values of J_2 and C_2 using (11) in the same way. For this experiment, we used the i30 of Hyundai Motors. Equation (14) is the result of fitting for each parameter, and Figs. 3 and 4 show a comparison between the experimental results and the transfer function by using a fitting value in the Bode plots

$$\begin{aligned} K &= 143.24 \text{ Nm/rad} \\ J_1 &= 0.044 \text{ kg} \cdot m^2, \quad C_1 = 0.25 \text{ Nm} \cdot \text{s/rad} \\ J_2 &= 0.11 \text{ kg} \cdot m^2, \quad C_2 = 1.35 \text{ Nm} \cdot \text{s/rad}. \end{aligned} \tag{14}$$

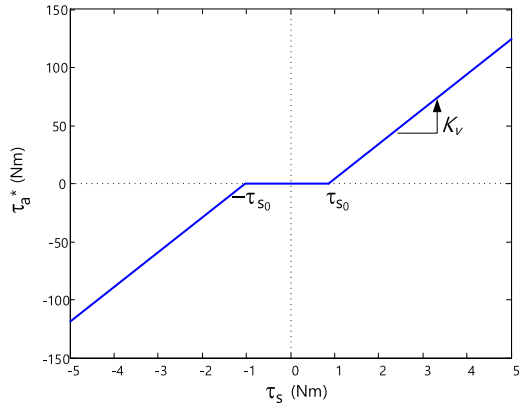

Fig. 5. Torque map of the EPS.

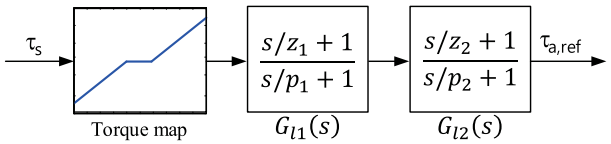

Fig. 6. Controller structure of the EPS.

III. Stability Analysis and Controller Design

A. Controller Structure

When the driver applies a steering torque to the steering wheel, the torque sensor measures the torque with (8) and outputs it to the controller of the EPS system. The EPS controller determines the assist torque of the motor after the measured torque passes through the torque map and compensator. We designed a typical steering characteristic map similar to Fig. 5 using (15). τ_a* is the assist torque value before it passes through the stabilizing compensator

$$\tau_a* = \begin{cases} 0, & 0 \le \tau_s \le \tau_{s_0} \\ K_v(v_{\text{car}})(\tau_s - \tau_{s_0}), & \tau_{s_0} < \tau_s. \end{cases} \tag{15}$$

The torque map has a deadband under τ_{s_0} to prevent the system from reacting too sensitively to driver torque, especially while driving at high speeds. This deadband is a source of nonlinearity of the controller. K_v decreases with increasing vehicle speed, because in the parking state, the driver requires a large assist torque, whereas less assist torque is necessary when driving at high speeds. The torque map applied on a conventional vehicle has a smoother curvilinear shape than Fig. 5, but for simplicity of analysis, we utilized a proportional function with a deadband.

The controller also needs some type of stabilizing compensator, because the high assist gain and nonlinearity of the torque map makes the system unstable. In this brief, we use a lead-lag compensator as a stabilizing filter so that the structure of the EPS controller resembles Fig. 6. The lead-lag compensator locates after the torque map and gives a dynamic characteristic to the controller while securing stability and suppressing vibration in the entire EPS system. The transfer function for the lead-lag compensator is

$$G_{li}(s) = \frac{s/z_i + 1}{s/p_i + 1}. \tag{16}$$

i in the subscript of the expression G_{li} indicates that several lead-lag compensators are used for the controller. The number of lead-lag compensators can increase with the need for a loop shaping. If $p_i > z_i$, then G_{li} is a lead compensator, and if $p_i < z_i$, then G_{li} is lag compensator. Generally, lead compensators increase the system phase margin to make it stable and lag compensators decrease the high frequency gain to prevent noise amplification. The pole and zero values of the lead-lag compensator that will be used for the controller are selected to satisfy the stable condition suggested in the next chapter.

B. Stability of the System With Approximate Linear Controller

When we approximate a torque map as a constant gain, the entire system containing the controller can be treated as a linear system, and we can analyze the stability of the linear system. When considering stability, the worst case is when the torque map is approximated as K_v, because the large gain can be source of system instability. The transfer function of the controller $H(s)$ can then be represented as

$$H(s) = K_v G_{l1}(s) G_{l2}(s) \cdots \tag{17}$$

We replace (7) and (18) into the system dynamics (1) and (6) and do a Laplace transform to obtain (19) and (20)

$$\tau_{a,\text{ref}} = H(s)\tau_s \tag{18}$$

$$(J_1 s^2 + C_1 s + K)\theta_1 - K\theta_2 = \tau_h \tag{19}$$

$$(J_2 s^2 + C_2 s + K + KHG_m)\theta_2 - (K + KHG_m)\theta_1 = -\tau_l. \tag{20}$$

With some modifications, the transfer function from the external system input (τ_h, τ_l) to the internal system output (θ_1, θ_2, τ_s) can be obtained

$$\theta_1 = \frac{P_1 + P_2 H}{1 + P_{\text{eq}} H}\tau_h + \frac{P_3}{1 + P_{\text{eq}} H}\tau_l \tag{21}$$

$$\theta_2 = \frac{P_4 + P_5 H}{1 + P_{\text{eq}} H}\tau_h + \frac{P_6}{1 + P_{\text{eq}} H}\tau_l \tag{22}$$

$$\tau_s = \frac{P_7}{1 + P_{\text{eq}} H}\tau_h + \frac{P_8}{1 + P_{\text{eq}} H}\tau_l. \tag{23}$$

$P_1 \sim P_8$ and P_{eq} are transfer function with system parameter and expression of each defined in the Appendix. It can be observed that all transfer function have common denominator, $1 + P_{\text{eq}} H$

$$1 + P_{\text{eq}} H = 0. \tag{24}$$

Equation (24) is characteristic equation that determines the stability of system and it is equivalent to the characteristic equation of the simple unity feedback system with plant $P_{\text{eq}}(s)$ and controller $H(s)$, as shown in Fig. 7 [13]. In linear control theory, robust stability of a unity feedback system can be obtained by a sufficient positive phase margin and gain margin of an open loop transfer function. If this is the case, the stability of the EPS system with an approximate linear

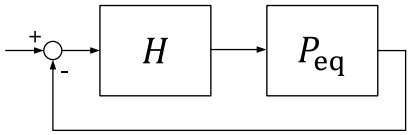

Fig. 7. Equivalent unity feedback system.

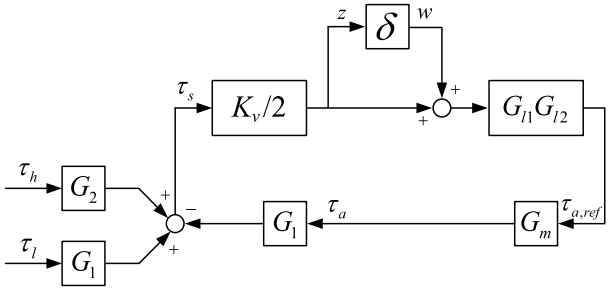

Fig. 8. System block diagram focusing on nonlinear controller.

torque map can be checked by the gain margin and the phase margin of $P_{\text{eq}}(s)H(s)$ [12]

$$\text{(Condition 1) } GM_{P_{\text{eq}}H} > 0, \;\; PM_{P_{\text{eq}}H} > 0. \tag{25}$$

C. Stability of the System With a Nonlinear Controller

Even if the stability of the system with a linearly approximated torque map is secured by satisfying Condition 1 (25), the system can still be unstable due to the nonlinearity of the torque map. The torque map can be expressed as a time-varying gain as observed in (26). The range can vary between 0 and K_v with variable δ that varies with time and has an absolute value that is always less than or equal to 1

$$\tau_a* = \tau_s \left(\frac{K_v}{2} + \frac{K_v}{2}\delta \right), \quad |\delta| \le 1. \tag{26}$$

Fig. 8 shows a rearrangement of the system block diagram, focusing on the controller with a time-varying gain. G_1 and G_2 represent transfer functions from system inputs(τ_a, τ_l, τ_h) to τ_s (27). Expressions G_1 and G_2 are described in the Appendix

$$\tau_s = G_2\tau_h - G_1\tau_a + G_1\tau_l. \tag{27}$$

If we combine all blocks, excluding δ, as one transfer function T_{zw}, the block diagram is reconstructed, as shown in Fig. 9.

According to small gain theory, a system loop will become stable when the amplitude of T_{zw} is less than 1 for any frequency range [11], [12]. Therefore, a new condition (28) is suggested for stability of the system with nonlinear torque map

$$\text{(Condition 2) } |T_{zw}(s)|_\infty < 1. \tag{28}$$

D. Lead-Lag Compensator Design

This section explains how to achieve compensator satisfying stability conditions suggested previously.

Compensator design is proceeded under the condition of parking state ($V_{car} = 0$), which is the worst case in terms of stability. Torque map has the steepest slope at parking state,

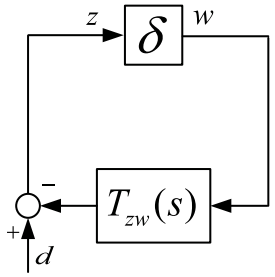

Fig. 9. Equivalent block diagram with T_{zw}.

because the largest assist torque is needed to cancel out friction between tire and road. This steep torque map provides large controller gain, which can be source of instability of closed-loop system. Therefore, if we design compensator for parking state, system will be stable for other velocity condition, which has smaller gain than parking state.

The Number of utilized lead compensator determine by how much phase should we secure at gain crossover frequency for sufficient phase margin of $P_{\text{eq}}H$. Utilizing more lead compensator provides larger phase lead, but also increases high frequency gain which makes system vulnerable to sensor noise. Phase margin of Bode plot of $P_{\text{eq}}H$ without lead-lag compensator can be criteria to determine number of lead compensator. Generally, system needs phase margin larger than 45° for robust stable condition and maximum phase that can be leaded by one lead compensator is limited to 55°. Therefore, if we want to elevate phase more than 55° near the gain crossover frequency, we need more than one lead compensator.

Second, lag compensator is used to prevent too high frequency gain caused by lead compensator and lowering gain crossover frequency, which helps lead compensator to obtain phase margin more efficiently. Lag compensator should be placed at frequency range lower than lead compensator not to cancel out the phase leading effect and higher than frequency of driver's steering command to prevent distortion of steering feel by phase lag. One lag compensator will be utilized for controller to support the phase leading of lead compensators and to reduce the high frequency gain.

We define the optimization problem to maximize cost function (29) with nonlinear constraints (28) and (30)

$$J(p_i, z_i) = a \cdot GM_{P_{\text{eq}}H} + b \cdot PM_{P_{\text{eq}}H} \tag{29}$$

$$p_{\min} < p_1 < z_1 < z_i < p_i < p_{\max} \quad (i = 2, 3, \ldots). \tag{30}$$

Cost function (29) is weighted sum of gain margin and phase margin of $P_{\text{eq}}H$ and constraint (30) limits range of poles and zeros of lead and lag compensator.

To obtain the optimum value of poles and zeros of compensator, we utilize "optimization toolbox" in MATLAB to solve nonlinear optimization problem.

IV. Simulation and Vehicle Test Result

A. Simulation Environment

The simulation environment is built with Simulink and consists of the EPS mechanism, controller, motor dynamics,

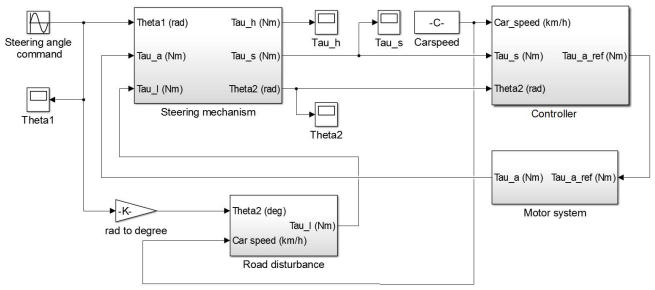

Fig. 10. Simulink simulation of EPS system.

TABLE III
SIMULATION AND OPTIMIZATION PARAMETERS

ω_m	100 Hz	τ_{s0}	2 Nm
K_v at parking state	35	Friction	2 Nm
a	0.1	b	1
p_{min}	6	p_{max}	1000

and road disturbance blocks as Fig. 10. The EPS mechanism, controller, and motor dynamics block are determined based on (1), (6), (10), (15), and (16). The steering angle is an input command for simulation. Gear friction between motor and column and between rack and pinion is also exerted as a coulomb friction to resemble real vehicle behavior. Last, road disturbance is divided in two different cases: the parking state and the driving state. In the parking state, road disturbance is a saturation function with hysteresis (31), and in the driving state, road disturbance is proportional to the steering angle (32) [14]. Parameters of torque map at parking state, actuator dynamics, and gear friction are listed at Table III. The rest of parameters of EPS system and road disturbance are based on system identification results (12) and the driving experiments

$$\begin{aligned} \tau_{l,k} &= K_{\text{tire,park}}(\theta_{2,k} - \theta_{t,k}) \\ \theta_{t,k} &= \begin{cases} \theta_{2,k} - \theta_{\max}, & \text{if } \theta_{2,k} - \theta_{t,k-1} > \theta_{\max} \\ \theta_{2,k} + \theta_{\max}, & \text{if } \theta_{2,k} - \theta_{t,k-1} > -\theta_{\max} \\ \theta_{t,k-1}, & \text{otherwise} \end{cases} \qquad (31) \\ \tau_{l,k} &= K_{\text{tire,drive}}\theta_{2,k}. \qquad (32) \end{aligned}$$

B. Controller Design Result and Simulation

Phase margin of $P_{\text{eq}}H$ without compensator (which means $H = K_v$) at the parking state is only $-15.7°$. Therefore, to secure enough phase margin (more than 45°), we decide to use two lead compensator for controller.

Parameters used in constraints and cost function are listed in Table III. Weighting parameters of cost function (29) are selected as Table III, because relatively larger value of the phase margin is needed than the gain margin and phase margin is more sensitive to the change of poles and zeros

Solution of the optimization problem is controller 4 of Table IV. Controllers 1–3 in Table IV are not optimal solution but selected to compared with optimized controller.

TABLE IV
POLE, ZERO, AND CONTROLLER DESIGN CONDITION PARAMETERS OF VARIOUS CONTROLLER CASES

Controller	1	2	3	4
p1	150	300	300	1000
z1	100	100	100	55.3
p2	1	1	5	6
z2	1	1	25	32.7
p3	1	1	1	713.0
z3	1	1	1	80.2
PM	-9.74 deg	2.05 deg	15.0 deg	56.4 deg
GM	-7.09 dB	0.89 dB	13.1 dB	11.2 dB
$\|T_{zw}(s)\|_\infty$	44.308	4.083	3.478	0.998

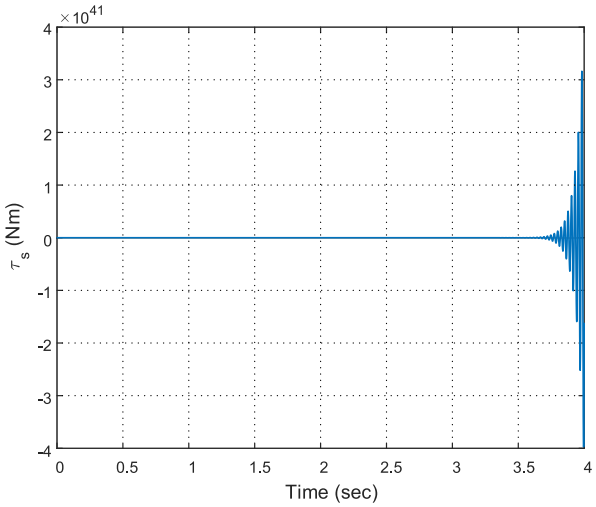

Fig. 11. Simulation result of controller 1.

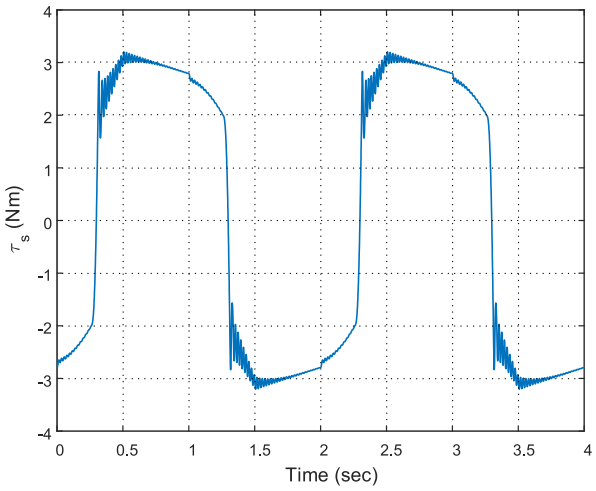

Fig. 12. Simulation result of controller 2.

EPS system with controllers at Table IV are simulated with steering angle commands of sine functions with an amplitude of 120° and a frequency of 0.5 Hz in the parking condition.

Fig. 11 shows a graph of the torque sensor value from the simulation with controller 1. Controller 1 does not satisfy both stability condition of approximately linear and nonlinear system, so system becomes unusable and diverge. Figs. 12 and 13

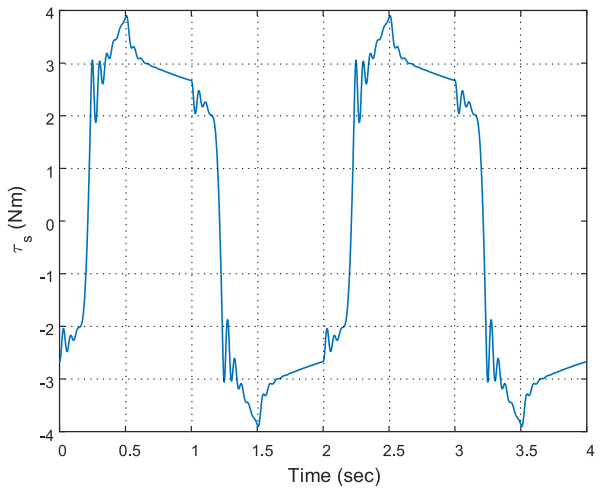

Fig. 13. Simulation result of controller 3.

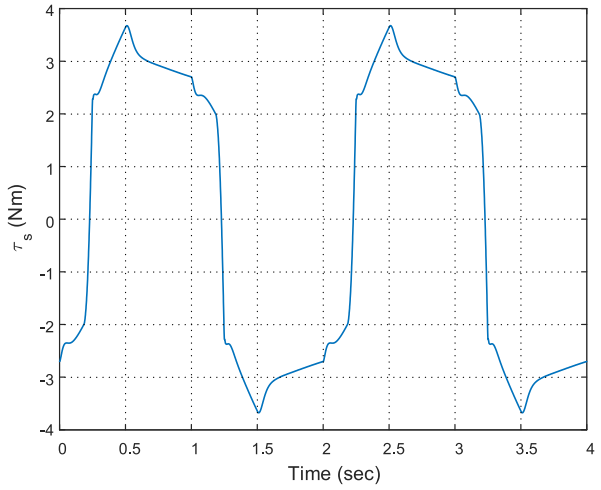

Fig. 14. Simulation result of controller 4.

show that even if a controller has positive phase margin and gain margin, if the controller has a high $\|T_{zw}(s)|_\infty$, vibration will occur in the system. This means that even though controller 2 makes approximately linear system stable, unstability of nonlinear element triggers vibration of system. The severity of the vibration is roughly proportional to the $|T_{zw}(s)|_\infty$ value. This tendency was consistent with various attempts of changing the pole and zero values of the controller. Finally, Fig. 14 shows that if the controller satisfies Conditions 1 and 2, the system is stable and no vibration is delivered to driver. Figs. 15 and 16 show Bode plots for the $P_{\mathrm{eq}}H$ and T_{zw} of controller 4.

C. Vehicle Test Result

The same vehicle used for model parameter identification is utilized for experiment and the experiment is performed while the vehicle is in parking condition. Controllers 3 and 4 in Table IV and torque map parameter in Table III are applied as controller of EPS system.

Figs. 17 and 18 show the experimental results of measuring steering angle and torque sensor value for each controller.

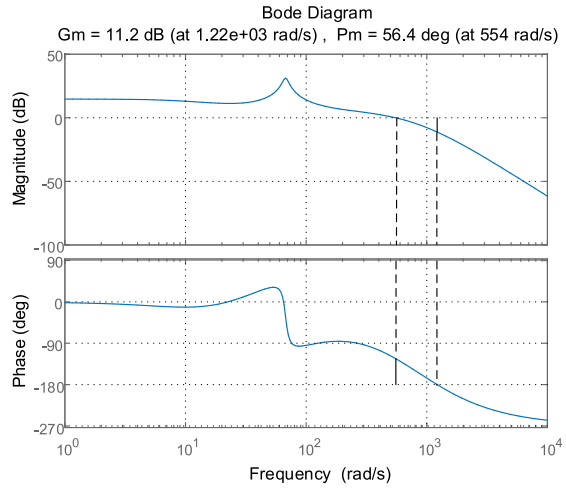

Fig. 15. Bode plot of $P_{\mathrm{eq}}H$ of controller 4.

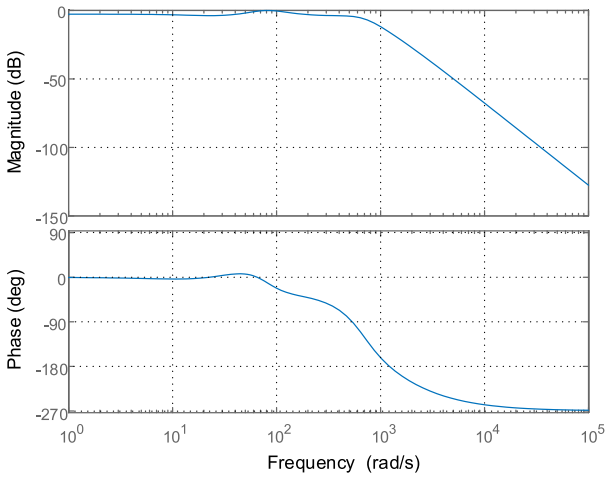

Fig. 16. Bode plot of T_{zw} of controller 4.

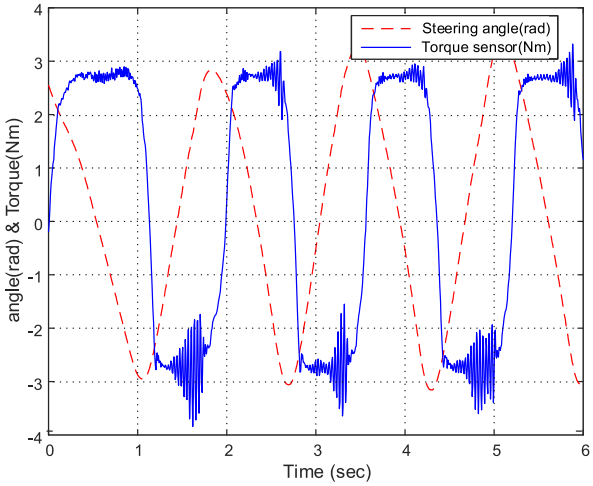

Fig. 17. Steering angle and torque sensor measurement of vehicle experiment with controller 3.

Controller 3 which satisfying positive phase and gain margin condition but not satisfying nonlinear system stability condition induces severe vibration. This vibration makes driver very

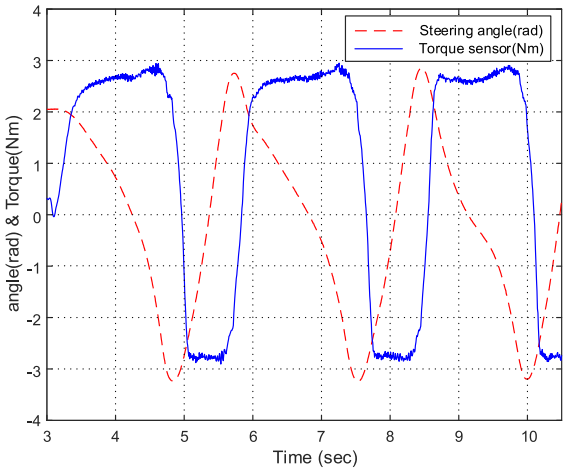

Fig. 18. Steering angle and torque sensor measurement of vehicle experiment with controller 4.

uncomfortable steering feel. On the other hand, controller 4 satisfying both stability condition induced very low amplitude of vibration (<0.3 Nm). The driver is unable to feel any discomfort due to vibration through the steering wheel with controller 4. The experiment results validate that a controller meeting both conditions makes the system stable with no critical vibration. In conclusion, suggested controller design method is well performed for real vehicle application.

V. Conclusion

This brief proposed an entire design process for a controller for an electric powered steering system based on the given torque map. This brief starts with modeling the EPS system and suggesting identification methods for system parameters. Then, design criteria for a stabilizing compensator for the controller are suggested to guarantee the stability of the system with an approximate linear controller and with a nonlinear controller. Optimization problem to find poles and zeros of lead-lag compensator is also suggested. Simulations show that the suggested analysis of the stability and controller design methods corresponds well with the results. Finally, the vehicle tests show that the designed controller performs well in a real vehicle.

Appendix

Transfer Function of $P_1 \sim P_8$, P_{eq}, G_1 and G_2

$$
\begin{aligned}
dom &= J_1J_2s^4 + (J_1C_2 + J_2C_1)s^3 \\
&\quad + (C_1C_2 + J_1K + J_2K)s^2 + (C_1K + C_2K)s \\
P_{eq}, P_8, G_1 &= K(J_1s^2 + C_1s)/\text{dom} \\
P_1 &= (J_2s^2 + C_2s + K)/\text{dom} \\
P_2, P_3, P_4, P_5 &= K/\text{dom} \\
P_6 &= (J_1s^2 + C_1s + K)/\text{dom} \\
P_7, G_2 &= K(J_2s^2 + C_2s)/\text{dom}
\end{aligned}
$$

References

[1] X. Chen, T. Yang, X. Chen, and K. Zhou, "A generic model-based advanced control of electric power-assisted steering systems," *IEEE Trans. Control Syst. Technol.*, vol. 16, no. 6, pp. 1289–1300, Nov. 2008.

[2] M. H. Lee, S. K. Ha, J. Y. Choi, and K. S. Yoon, "Improvement of the steering feel of an electric power steering system by torque map modification," *J. Mech. Sci. Technol.*, vol. 19, no. 3, pp. 792–801, 2005.

[3] N. Sugitani, Y. Fujuwara, K. Uchida, and M. Fujita, "Electric power steering with H-infinity control designed to obtain road information," in *Proc. Amer. Control Conf.*, vol. 5. Jun. 1997, pp. 2935–2939.

[4] A. Marouf, M. Djemai, C. Sentouh, and P. Pudlo, "A new control strategy of an electric-power-assisted steering system," *IEEE Trans. Veh. Technol.*, vol. 61, no. 8, pp. 3574–3589, Oct. 2012.

[5] A. T. Zaremba, M. K. Liubakka, and R. M. Stuntz, "Control and steering feel issues in the design of an electric power steering system," in *Proc. Amer. Control Conf.*, vol. 1, Jun. 1998, pp. 36–40.

[6] M. Kurishige, O. Nishihara, and H. Kumamoto, "A new control strategy to reduce steering torque without perceptible vibration for vehicles equipped with electric power steering," *J. Vibrat. Acoust.-Trans. Asme*, vol. 132, no. 5, p. 054504, Oct. 2010.

[7] R. C. Chabaan and L. Y. Wang, "Control of electrical power assist systems: $H\infty$ design, torque estimation and structural stability," *JSAE Rev.*, vol. 22, no. 4, pp. 435–444, 2001.

[8] A. Marouf, C. Sentouh, M. Djemai, and P. Pudlo, "Control of electric power assisted steering system using sliding mode control," in *Proc. 14th Int. IEEE Conf. Intell. Transp. Syst. (ITSC)*, Oct. 2011, pp. 107–112.

[9] M. Parmar and J. Y. Hung, "A sensorless optimal control system for an automotive electric power assist steering system," *IEEE Trans. Ind. Electron.*, vol. 51, no. 2, pp. 290–298, Apr. 2004.

[10] H. B. Pacejka, *Tyre and Vehicle Dynamics*, 2nd ed. Warrendale, PA, USA: SAE International, 2006.

[11] H. K. Khalil, *Nonlinear Systems*, 3rd ed. Upper Saddle River, NJ, USA: Prentice Hall, 2000.

[12] G. F. Franklin, J. D. Powell, and A. Emami-Naeini, *Feedback Control of Dynamic Systems*, 6th ed. Upper Saddle River, NJ, USA: Pearson Education, 2010.

[13] K. A. Morris, *Introduction to Feedback Control*. London, U.K.: Academic, 2001.

[14] A. Zaremba and R. I. Davis, "Dynamic analysis and stability of a power assist steering system," in *Proc. Amer. Control Conf.*, vol. 6. Jun. 1995, pp. 4253–4257.